The Journal of Chemical Physics

Systematic description of molecular deformations with Cremer–Pople puckering and deformation coordinates utilizing analytic derivatives: Applied to cycloheptane, cyclooctane, and cyclo[18]carbon

Cite as: J. Chem. Phys. **152**, 154107 (2020); https://doi.org/10.1063/1.5144278
Submitted: 30 December 2019 . Accepted: 21 February 2020 . Published Online: 20 April 2020

Wenli Zou, Yunwen Tao, and Elfi Kraka

AIP Publishing

The Journal of Chemical Physics ARTICLE scitation.org/journal/jcp

Systematic description of molecular deformations with Cremer–Pople puckering and deformation coordinates utilizing analytic derivatives: Applied to cycloheptane, cyclooctane, and cyclo[18]carbon

Cite as: J. Chem. Phys. 152, 154107 (2020); doi: 10.1063/1.5144278
Submitted: 30 December 2019 • Accepted: 21 February 2020 •
Published Online: 20 April 2020

Wenli Zou,[1,2] Yunwen Tao,[1] and Elfi Kraka[1,a)]

AFFILIATIONS

[1]Computational and Theoretical Chemistry Group (CATCO), Department of Chemistry, Southern Methodist University, 3215 Daniel Ave., Dallas, Texas 75275-0314, USA
[2]Institute of Modern Physics, Northwest University, and Shaanxi Key Laboratory for Theoretical Physics Frontiers, Xi'an, Shaanxi 710127, People's Republic of China

[a)]**Author to whom correspondence should be addressed:** ekraka@smu.com

ABSTRACT

The conformational properties of ring compounds such as cycloalkanes determine to a large extent their stability and reactivity. Therefore, the investigation of conformational processes such as ring inversion and/or ring pseudorotation has attracted a lot of attention over the past decades. An in-depth conformational analysis of ring compounds requires mapping the relevant parts of the conformational energy surface at stationary and also at non-stationary points. However, the latter is not feasible by a description of the ring with Cartesian or internal coordinates. We provide in this work, a solution to this problem by introducing a new coordinate system based on the Cremer–Pople puckering and deformation coordinates. Furthermore, analytic first- and second-order derivatives of puckering and deformation coordinates, i.e., B-matrices and D-tensors, were developed simplifying geometry optimization and frequency calculations. The new coordinate system is applied to map the potential energy surfaces and reaction paths of cycloheptane (C_7H_{14}), cyclooctane (C_8H_{16}), and cyclo[18]carbon (C_{18}) at the quantum chemical level and to determine for the first time all stationary points of these ring compounds in a systematic way.

I. INTRODUCTION

Theoretical chemists generally prefer the use of Cartesian coordinates when solving the Schrödinger or Dirac equation in some approximate way. This results from the fact that the electron integrals and their derivatives can be efficiently calculated in terms of Cartesian coordinates and that there is always a unique set of 3N Cartesian Coordinates for a system being composed of N atoms. On the other hand, experimentally oriented chemists generally prefer to describe molecular geometries in terms of internal coordinates, such as bond lengths, bond angles, and dihedral angles, because they are more intuitive.[1] However, there is no unique set of $(3N - N_{tr})$ internal coordinates, with $N_{tr} = 6$ for nonlinear and 5 for linear polyatomic molecules. This often leads to the question, which internal coordinates are best suited for the description of the molecular system under consideration.[2] The basic equation of vibrational spectroscopy is defined in Cartesian coordinates.[3] However, it can be extended to internal coordinates using the well-known Wilson B-matrix formalism, which connects internal or other coordinates (e.g., symmetry coordinates) to Cartesian coordinates via the first

order derivatives of the internal coordinates with regard to Cartesian coordinates.[3–5] This formalism is at the heart of modern vibrational spectroscopy[6,7] and has been realized in an increasing number of algorithms, such as the natural extension reference frame algorithm[8] or even involving machine learning procedures,[9] just to name a few.

Despite their popularity, both Cartesian and internal coordinates are no longer an optimal choice for the description of reacting molecules. As the atoms of a molecule move on curved paths in such a situation, the dynamics of a molecule is better described in terms of curvilinear coordinates.[10,11] In computational chemistry, the deficiency of internal coordinates can be alleviated to some extent by using redundant sets of internal coordinates,[12–15] which help us to at least approximately describe the curved paths of the atoms during geometry optimization.[16–19] However, these approximations tend to fail for the description of vibrating molecules,[20,21] and for the description of ring systems and their conformational changes,[22–24] or in more general terms, when a dynamic process of a molecule has to be described in a precisely defined space. For example, the conformational space of a puckered N-membered ring ($N - ring$) is spanned by N − 3 coordinates,[24,25] the Jahn–Teller surface for bond pseudorotation by 2N − 3 coordinates, which contains N − 2 two-dimensional subspaces,[22] the space of the Berry pseudorotation of an AB_5 system is 2-dimensional[26] as well as that of the corresponding turnstile pseudorotation.[27] In all these cases, it is not clear which internal coordinates should be used to determine the corresponding conformational energy surface (CES). The geometry of a puckered N-ring might be described by N ring bonds, N − 3 internal ring angles, and N − 3 dihedral angles. Since there is no unique way of selecting N − 3 angles out of a set of N possible angles, the question which is the best set of internal coordinates to be used for specifying the geometry of a puckered N-ring cannot be answered. The stationary points on the CES can be determined using redundant internal coordinates. However, in order to map the relevant parts of the CES, which describe conformational processes such as ring inversion and/or ring pseudorotation with quantum chemical means, one has to investigate also conformations at non-stationary points of the CES. This is not feasible by the description of the ring with Cartesian or internal coordinates.[28] A solution to this problem is provided by using the Cremer–Pople puckering coordinates[24,28–30] that specify the pucker of an N-ring by N − 3 uniquely defined puckering coordinates that split up into (N − 3)/2 puckering amplitude–pseudorotation phase angle pairs q_n, ϕ_n with $n = 2, \ldots, (N - 1)/2$ for N being odd and $n = 2, \ldots, (N - 2)/2$ and a single puckering amplitude $q_{N/2}$ describing crown-puckering for N being even. Using N bond lengths, N − 3 bond angles, and the N − 3 puckering coordinates any conformer of an N-ring located at a non-stationary point of the CES can be described by a constrained geometry optimization. The advantages of describing ring pseudorotation and ring inversion with the help of Cremer–Pople puckering coordinates are amply documented in the literature.[22,23,31–45]

There remains still some arbitrariness when selecting the N bond lengths and N − 3 bond angles complementing the N − 3 puckering coordinates. This arbitrariness vanishes when complementing the puckering coordinates by a set of 2N − 3 ring deformation coordinates.[22,23,40] These coordinates specify the geometry of the planar ring form in terms of deformation amplitudes t_n and deformation phase angles τ_n with $n = 1, \ldots, (N - 2)$ for N odd or even and a single ring radius $R = R_0 + t_0$ changing from the value R_0 for a regular N-membered polygon (N-gon) with D_{Nh} symmetry upon a breathing deformation of the N-gon with amplitude t_0. Using N − 3 puckering and 2N − 3 deformation coordinates, which we will call ring puckering and deformation (RPD) coordinates in the following, the geometry of any planar or puckered N-ring can be uniquely defined, which is of outmost relevance for the determination of the geometry of specified pucker and/or deformations, the analysis of pucker and deformation in substituted N-rings, and the investigation of dynamic processes such as ring inversion, ring pseudorotation, bond pseudorotation in Jahn–Teller systems, bond shifting in annulenes, etc.

The manuscript is structured as follows: In Sec. II, we introduce the theory of RPD coordinates for any N-ring system, including analytic first and second derivatives. The implementation of RPD coordinates is discussed in Sec. III. In Sec. IV, we apply our new coordinates to describe the puckering of cycloheptane and cyclooctane as representative examples for odd and even-numbered N-rings, respectively, and also to explore the deformation of the recently synthesized cyclo[18]carbon.[46] Conclusions, including a summary of the advantages of using RPD coordinates, are drawn in Sec. V.

II. THEORY

A. RPD coordinates

The coordinates of an N-ring can be defined with regard to an arbitrary orientation of the coordinate system. However, for the calculation of the puckering and deformation coordinates, a special orientation (called "standard orientation") has to be adopted. This is defined by using the xy-plane as the mean plane of the N-ring and defining the norm to the mean plane as the +z-axis (unit vector $\mathbf{e}_z$). The mean plane contains the planar reference ring of the puckered N-ring obtained by setting all puckering amplitudes $q_n = 0$. The geometrical center of the planar reference ring is taken as the origin of the Cartesian coordinate system and atom 1 of the planar reference ring is positioned on the negative x-axis in the *9 o'clock* position.

In the following, we will use the letter of the Greek alphabet for atomic numbers in the clockwise direction, including (1) atomic number α (= 1, . . ., N) in an arbitrary initial orientation, (2) atomic number β (= 1, . . ., N) in the standard orientation of RPD coordinates, and (3) $\gamma \equiv \beta - 1$. When needed, r_α^l (l = 1, 2, and 3 for x, y, and z) will be used for the Cartesian coordinates $(x_\alpha, y_\alpha, z_\alpha) \equiv \mathbf{r}_\alpha$ of atom α, and r_β^k (k = 1, 2, and 3 for x, y, and z) for the Cartesian coordinates $(x_\beta, y_\beta, z_\beta) \equiv \mathbf{r}_\beta$ of atom β, respectively.

The geometrical center of the N-ring being the origin of the Cartesian coordinate system is imposed by

$$\sum_\alpha r_\alpha^l = 0 \tag{1}$$

and the mean plane is determined with the help of two auxiliary vectors $\mathbf{R}'$ and $\mathbf{R}''$ that span the xy-plane

$$\mathbf{R}' = \sum_\alpha \mathbf{r}_\alpha \sin\zeta_\alpha, \tag{2}$$

$$\mathbf{R}'' = \sum_\alpha \mathbf{r}_\alpha \cos\zeta_\alpha, \tag{3}$$

where

$$\zeta_\alpha = \frac{2\pi(\alpha - 1)}{N}. \tag{4}$$

The unit vector in the z-direction (normal to the mean plane), $\mathbf{e}_z$, is calculated as

$$\mathbf{e}_z = \frac{\mathbf{R}' \times \mathbf{R}''}{|\mathbf{R}' \times \mathbf{R}''|}, \tag{5}$$

and for x- and y-components, the unit vectors $\mathbf{e}_x$ and $\mathbf{e}_y$ may be determined by

$$\mathbf{e}_x = \frac{\mathbf{e}_z(\mathbf{r}_1^0, \mathbf{e}_z) - \mathbf{r}_1^0}{|\mathbf{e}_z(\mathbf{r}_1^0, \mathbf{e}_z) - \mathbf{r}_1^0|} = -\frac{\mathbf{R}'' + \mathbf{e}_z \times \mathbf{R}'}{|\mathbf{R}'' + \mathbf{e}_z \times \mathbf{R}'|} = -\frac{\mathbf{u}}{|\mathbf{u}|}, \tag{6}$$

and $\mathbf{e}_y = \mathbf{e}_z \times \mathbf{e}_x$, where $\mathbf{r}_1^0$ is the position of the first atom in the reference N-gon (in standard orientation),

$$\mathbf{r}_1^0 = \frac{1}{N} \sum_{\beta'} \mathbf{C}^\beta \ \mathbf{r}_{\beta'}, \tag{7}$$

and $\mathbf{C}^\beta$ describes counter-clockwise rotation by $\eta_\gamma \equiv \eta_\gamma^{(0)} = 2\pi\gamma/N$ [cf. Eq. (19)] around $\mathbf{e}_z$,

$$\mathbf{C}^\beta \ \mathbf{r}_{\beta'} = \mathbf{r}_{\beta'} \cos\eta_\gamma + (\mathbf{e}_z \times \mathbf{r}_{\beta'}) \sin\eta_\gamma + \mathbf{e}_z(\mathbf{e}_z, \mathbf{r}_{\beta'})(1 - \cos\eta_\gamma). \tag{8}$$

The above three unit vectors $\mathbf{e}_x$, $\mathbf{e}_y$, and $\mathbf{e}_z$ determine a unique standard orientation, and the corresponding Cartesian coordinates can be computed by

$$r_\beta^k = \mathbf{r}_\beta \cdot \mathbf{e}_k \equiv (\mathbf{r}_\beta, \mathbf{e}_k). \tag{9}$$

Hence, for any puckered ring, the choice of the origin and the mean plane impose

$$\sum_\beta r_\beta^k = 0 \tag{10}$$

and

$$\sum_\beta z_\beta \cos\zeta_\beta = 0, \tag{11}$$

$$\sum_\beta z_\beta \sin\zeta_\beta = 0. \tag{12}$$

The puckering coordinates are defined by

$$q_n \cos\phi_n = \sqrt{\frac{2}{N}} \sum_\beta z_\beta \cos\omega_\gamma^{(n)}, \tag{13}$$

$$q_n \sin\phi_n = -\sqrt{\frac{2}{N}} \sum_\beta z_\beta \sin\omega_\gamma^{(n)}, \tag{14}$$

with

$$\omega_\gamma^{(n)} = \frac{2\pi n\gamma}{N}, \tag{15}$$

for $n = 2, \ldots, N/2 - 1$ (N even) or $n = 2, \ldots, (N-1)/2$ (N odd). For even N, an additional ring puckering amplitude describing crown puckering is given by

$$q_{N/2} = \sqrt{\frac{1}{N}} \sum_\beta z_\beta \cos(\gamma\pi) = \sqrt{\frac{1}{N}} \sum_\beta (-1)^\gamma z_\beta. \tag{16}$$

The deformation coordinates of a planar N-ring are defined by Eqs. (17) and (18)[22]

$$t_n \cos\tau_n = \frac{1}{N} \sum_\beta \left(x_\beta \cos\eta_\gamma^{(n)} - y_\beta \sin\eta_\gamma^{(n)} \right), \tag{17}$$

$$t_n \sin\tau_n = \frac{1}{N} \sum_\beta \left(x_\beta \sin\eta_\gamma^{(n)} + y_\beta \cos\eta_\gamma^{(n)} \right), \tag{18}$$

with

$$\eta_\gamma^{(n)} = \frac{2\pi(n+1)\gamma}{N}, \tag{19}$$

where $n = 0, \cdots, N-2$ but t_0 (i.e., radius R; also called breathing amplitude) does not have a phase angle τ_0.

Using the above formulas, the puckering and deformation coordinates can be determined from the Cartesian coordinates of an arbitrary ring molecule only if the atoms are correctly ordered.

For a given set of RPD coordinates, the corresponding Cartesian coordinates can be extracted according to

$$x_\beta = -R\cos\eta_\gamma^{(0)} + \sum_{n=1}^{N-2} t_n \cos\left(\tau_n - \eta_\gamma^{(n)}\right), \tag{20}$$

$$y_\beta = R\sin\eta_\gamma^{(0)} + \sum_{n=1}^{N-2} t_n \sin\left(\tau_n - \eta_\gamma^{(n)}\right), \tag{21}$$

for x- and y-coordinates, respectively, and

$$z_\beta = \sqrt{\frac{2}{N}} \sum_{n=2}^{(N-1)/2} q_n \cos\left(\phi_n + \omega_\gamma^{(n)}\right) \quad \text{(N odd)}, \tag{22}$$

$$z_\beta = \sqrt{\frac{2}{N}} \sum_{n=2}^{(N-2)/2} q_n \cos\left(\phi_n + \omega_\gamma^{(n)}\right) + \sqrt{\frac{1}{N}} q_{N/2} (-1)^\gamma \quad \text{(N even)}, \tag{23}$$

for z-coordinates of atom β. The translational ($\mathcal{T}$) and rotational ($\mathcal{R}$) modes in RPD coordinates may be obtained by the generalization of Eqs. (20)–(22), i.e., $\{t_{n-1}, \tau_{n-1} = 0 \text{ or } \pi/2\}$ for $\mathcal{T}_x$ or $\mathcal{T}_y$, $\{t_0, \tau_0 = \pi/2\}$ for $\mathcal{R}_z$, $\{q_1, \phi_1 = 0 \text{ or } \pi/2\}$ for $\mathcal{R}_y$ or $\mathcal{R}_x$, and $\{q_0, \phi_0 = 0\}$ for $\mathcal{T}_z$, whereas, $\{q_0, \phi_0 = \pi/2\}$ does not change the geometry.

B. First derivatives of RPD coordinates

The equilibrium geometry of an N-ring corresponds to that point on the CES, for which all internal coordinate forces f_q (q: bond lengths, bond angles, and dihedral angles) vanish. Accurate geometry optimizations are based on the determination of the analytic energy gradient that collects all forces f_q. Analytical energy gradients with regard to Cartesian coordinates r_α^l are available for most quantum chemical methods. The transformation of Cartesian coordinates r_α^l and Cartesian coordinate forces f_r into internal coordinates q and internal coordinate forces f_q, respectively, can be accomplished via the use of the Wilson B-matrix.[3] The infinitesimal displacements

$\Delta\mathbf{q}$ are related to the corresponding Cartesian displacements $\Delta\mathbf{r}$ by the appropriate Wilson B-matrix elements[3]

$$\Delta\mathbf{q} = \mathbf{B}\Delta\mathbf{r}, \tag{24}$$

where

$$B^n_{\alpha,l} = \frac{\partial q_n}{\partial r^l_\alpha}. \tag{25}$$

Transformation of the forces f_r collected in the gradient $\mathbf{g}_r$ requires the pseudo-inverse of $\mathbf{B}$,

$$\mathbf{g}_q = \mathbf{A}^\dagger \mathbf{g}_r, \tag{26}$$

with

$$\mathbf{A} = \mathbf{W}^{-1}\mathbf{B}^\dagger(\mathbf{B}\mathbf{W}^{-1}\mathbf{B}^\dagger)^{-1}, \tag{27}$$

where $\mathbf{W}$ is an arbitrary non-singular 3N × 3N square matrix. For the Hessian in internal coordinates, $\mathbf{W} = \mathbf{M}$ ($\mathbf{M}$ is the mass matrix) is usually used,[14,47] but in geometry optimizations, the identity matrix is often taken[15] for $\mathbf{W}$ to utilize massless dummy atoms.

For the purpose of extending standard internal coordinates to RPD coordinates and optimizing the geometry of an N-ring in RPD coordinates, the following B-matrix elements have to be determined:

$$B^n_{\alpha,l} = \sum_{\beta,k} \frac{\partial \xi_n}{\partial r^k_\beta}\frac{\partial r^k_\beta}{\partial r^l_\alpha}, \tag{28}$$

where ξ_n can be either puckering coordinates $\{q_n, \phi_n\}$ or deformation coordinates $\{t_n, \tau_n\}$. Equation (28) may also be expressed in a matrix form $\mathbf{b}_n = \mathbf{b}^*_n\mathbf{\Delta}$, where $\mathbf{b}^*_n$ is a row vector of B-matrix for ξ_n in the standard orientation, and the $3N \times 3N$ matrix $\mathbf{\Delta}$ is the response of the Cartesian coordinates in standard orientation to the ones in initial orientation.

The B-matrix of puckering coordinates was originally derived in Ref. 28 and recently revisited in Ref. 48 by deriving Eqs. (13), (14) and (16) regard to z_β

$$\frac{\partial q_n}{\partial z_\beta} = \sqrt{\frac{2}{N}}\cos\left(\omega^{(n)}_\gamma + \phi_n\right), \tag{29}$$

$$\frac{\partial \phi'_n}{\partial z_\beta} = q_n\frac{\partial \phi_n}{\partial z_\beta} = -\sqrt{\frac{2}{N}}\sin\left(\omega^{(n)}_\gamma + \phi_n\right), \tag{30}$$

along with $\partial q_{N/2}/\partial z_\beta = (-1)^\gamma/\sqrt{N}$ for an even N-ring. In Eq. (30), $\partial\phi_n/\partial z_\beta$ is replaced by $\partial\phi'_n/\partial z_\beta$ to avoid numerical instability if q_n is small or zero at some geometries; in this case, ϕ_n can be an arbitrary value, and one may just take $\partial\phi_n/\partial z_\alpha = 0$.

Differentiating Eqs. 17 and 18 except for $n = 0$ with regard to x_β and y_β, the B-matrix entries for deformation coordinates are obtained,

$$\frac{\partial t_n}{\partial x_\beta} = \frac{1}{N}\cos\left(\tau_n - \eta^{(n)}_\gamma\right), \tag{31}$$

$$\frac{\partial t_n}{\partial y_\beta} = \frac{1}{N}\sin\left(\tau_n - \eta^{(n)}_\gamma\right), \tag{32}$$

$$\frac{\partial \tau'_n}{\partial x_\beta} = t_n\frac{\partial \tau_n}{\partial x_\beta} = -\frac{1}{N}\sin\left(\tau_n - \eta^{(n)}_\gamma\right), \tag{33}$$

$$\frac{\partial \tau'_n}{\partial y_\beta} = t_n\frac{\partial \tau_n}{\partial y_\beta} = \frac{1}{N}\cos\left(\tau_n - \eta^{(n)}_\gamma\right). \tag{34}$$

Again, we take $\partial\tau'_n/\partial x_\beta$ and $\partial\tau'_n/\partial y_\beta$ for better numerical stability, thus $\partial\tau_n/\partial x_\beta = \partial\tau_n/\partial y_\beta = 0$ for small t_n.

The B-matrix entry of the radius $R \equiv t_0$ has to be derived separately since the corresponding phase angle τ_0 does not exist, which is

$$\frac{\partial R}{\partial \mathbf{r}^k_\beta} = \frac{1}{N^2 R}\sum_{\beta'}\mathbf{C}^{\beta'-\beta}\ \mathbf{r}_{\beta'}. \tag{35}$$

In Eq. (35), the following abbreviated form has been used for simplification:

$$\left(\frac{\partial}{\partial x_\alpha}, \frac{\partial}{\partial y_\alpha}, \frac{\partial}{\partial z_\alpha}\right) = \frac{\partial}{\partial \mathbf{r}_\alpha}, \tag{36}$$

and similarly a symbol for the second-order derivative $\partial^2/\partial\mathbf{r}_\alpha\partial\mathbf{r}_{\alpha'}$ (see Subsection II C) may also be defined, which is a 3 × 3 matrix.

Equations 29–35 define the first term on the right-hand-side (*rhs.*) in Eq. (28) for RPD coordinates, whereas the second term may be calculated by derivation of Eq. (9), leading to

$$\frac{\partial z_\beta}{\partial \mathbf{r}_\alpha} = (\mathbf{e}_z, \mathbf{I})\ \delta_{\alpha\beta} + \left(\mathbf{r}_\beta, \frac{\partial \mathbf{e}_z}{\partial \mathbf{r}_\alpha}\right), \tag{37}$$

with $\mathbf{I}$ being the 3 × 3 identity matrix and

$$\frac{\partial \mathbf{e}_z}{\partial \mathbf{r}_\alpha} = \frac{1}{|\mathbf{R}' \times \mathbf{R}''|}\left(\mathbf{a}''\ \sin\zeta_\alpha - \mathbf{a}'\ \cos\zeta_\alpha\right), \tag{38}$$

where

$$\mathbf{a} = \mathbf{I} \times \mathbf{R} - \mathbf{e}_z(\mathbf{I} \times \mathbf{R}, \mathbf{e}_z), \tag{39}$$

with $\mathbf{a} = \mathbf{a}'$ or $\mathbf{a}''$ and $\mathbf{R} = \mathbf{R}'$ or $\mathbf{R}''$, and

$$\mathbf{I} \times \mathbf{R} = \begin{bmatrix} 0 & R_z & -R_y \\ -R_z & 0 & R_x \\ R_y & -R_x & 0 \end{bmatrix}. \tag{40}$$

The derivatives of $\mathbf{e}_x$ and $\mathbf{e}_y$ with regard to r^l_α are

$$\frac{\partial \mathbf{e}_x}{\partial \mathbf{r}_\alpha} = \frac{1}{|\mathbf{u}|}\left[\mathbf{e}_x\left(\mathbf{e}_x, \frac{\partial \mathbf{u}}{\partial \mathbf{r}_\alpha}\right) - \frac{\partial \mathbf{u}}{\partial \mathbf{r}_\alpha}\right], \tag{41}$$

with

$$\frac{\partial \mathbf{u}}{\partial \mathbf{r}_\alpha} = \mathbf{I}\ \cos\eta_\alpha + \frac{\partial \mathbf{e}_z}{\partial \mathbf{r}_\alpha} \times \mathbf{R}' + \mathbf{e}_z \times \mathbf{I}\ \sin\eta_\alpha. \tag{42}$$

This leads to the derivative of x_β with regard to r^l_α:

$$\frac{\partial x_\beta}{\partial \mathbf{r}_\alpha} = (\mathbf{e}_x, \mathbf{I})\ \delta_{\alpha\beta} + \left(\frac{\partial \mathbf{e}_x}{\partial \mathbf{r}_\alpha}, \mathbf{r}_\beta\right). \tag{43}$$

Similar formulas may be obtained for the y-component,

$$\frac{\partial y_\beta}{\partial \mathbf{r}_\alpha} = (\mathbf{e}_y, \mathbf{I})\ \delta_{\alpha\beta} + \left(\frac{\partial \mathbf{e}_y}{\partial \mathbf{r}_\alpha}, \mathbf{r}_\beta\right), \tag{44}$$

where

$$\frac{\partial \mathbf{e}_y}{\partial \mathbf{r}_\alpha} = \frac{\partial \mathbf{e}_z}{\partial \mathbf{r}_\alpha} \times \mathbf{e}_x + \mathbf{e}_z \times \frac{\partial \mathbf{e}_x}{\partial \mathbf{r}_\alpha}. \tag{45}$$

The above equations provide all necessary formulas for constituting the B-matrix of a ring molecule.

C. Second derivatives of RPD coordinates

Using the B-matrix in terms of RPD coordinates as described in Subsection II B, geometry optimization in terms of RPD coordinates is principally possible. However, in some advanced optimization methods like quasi-Newton and Newton–Raphson Schemes,[49] a transformation of Cartesian Hessians $\mathbf{F}_r$ into internal coordinate Hessians $\mathbf{F}_q$ is necessary.[12,15]

$$\mathbf{F}_q = \mathbf{A}^\dagger \mathbf{F}_r \mathbf{A} - \sum_n g_{q,n} \mathbf{A}^\dagger \mathbf{D}_n \mathbf{A}. \tag{46}$$

In addition to the inverse of Wilson's B-matrix (**A**), a D-tensor of **B** derivatives (**D**) is also involved in Eq. (46), which is also called **B′** or **C** in the literature.[12,14,15] The second derivatives of RPD coordinates ξ_n with regard to Cartesian coordinates r^l_α are given by

$$D^n_{(\alpha,l),(\alpha',l')} := \frac{\partial^2 \xi_n}{\partial r^l_\alpha \partial r^{l'}_{\alpha'}} = \sum_{\beta,\beta',k,k'} \frac{\partial^2 \xi_n}{\partial r^k_\beta \partial r^{k'}_{\beta'}} \frac{\partial r^k_\beta}{\partial r^l_\alpha} \frac{\partial r^{k'}_{\beta'}}{\partial r^{l'}_{\alpha'}} + \sum_{\beta,i} \frac{\partial \xi_n}{\partial r^k_\beta} \frac{\partial^2 r^k_\beta}{\partial r^l_\alpha \partial r^{l'}_{\alpha'}}. \tag{47}$$

Nine types of second derivatives $\partial^2 \xi_n / \partial r^k_\beta \partial r^{k'}_{\beta'}$ in Eq. (47) have to be derived to obtain the D-tensor being necessary for the transformation from Cartesian to RPD coordinates. For the ring puckering coordinates $\{q_n, \phi_n\}$ these are

$$\frac{\partial^2 q_n}{\partial z_\beta \partial z_{\beta'}} = \frac{2}{N q_n} \sin(\omega^{(n)}_\gamma + \phi_n) \sin(\omega^{(n)}_{\gamma'} + \phi_n), \tag{48}$$

$$\frac{\partial^2 \phi_n}{\partial z_\beta \partial z_{\beta'}} = \frac{2}{N q_n^2} \sin(\omega^{(n)}_\gamma + \omega^{(n)}_{\gamma'} + 2\phi_n), \tag{49}$$

where $\omega^{(n)}_\gamma$ has been defined in Eq. (15). For $q_{N/2}$ of even N-membered ring, its D-tensor is always zero.

For the planar deformation coordinates except for $n = 0$, the corresponding second derivatives are

$$\frac{\partial^2 t_n}{\partial x_\beta \partial x_{\beta'}} = \frac{1}{N^2 t_n} \sin(\tau_n - \eta^{(n)}_\gamma) \sin\left(\tau_n - \eta^{(n)}_{\gamma'}\right), \tag{50}$$

$$\frac{\partial^2 t_n}{\partial x_\beta \partial y_{\beta'}} = \frac{-1}{N^2 t_n} \sin(\tau_n - \eta^{(n)}_\gamma) \cos\left(\tau_n - \eta^{(n)}_{\gamma'}\right), \tag{51}$$

$$\frac{\partial^2 t_n}{\partial y_\beta \partial y_{\beta'}} = \frac{1}{N^2 t_n} \cos(\tau_n - \eta^{(n)}_\gamma) \cos\left(\tau_n - \eta^{(n)}_{\gamma'}\right), \tag{52}$$

$$\frac{\partial^2 \tau_n}{\partial x_\beta \partial x_{\beta'}} = \frac{1}{N^2 t_n^2} \sin\left(2\tau_n - \eta^{(n)}_\gamma - \eta^{(n)}_{\gamma'}\right), \tag{53}$$

$$\frac{\partial^2 \tau_n}{\partial x_\beta \partial y_{\beta'}} = \frac{-1}{N^2 t_n^2} \cos\left(2\tau_n - \eta^{(n)}_\gamma - \eta^{(n)}_{\gamma'}\right), \tag{54}$$

$$\frac{\partial^2 \tau_n}{\partial y_\beta \partial y_{\beta'}} = \frac{-1}{N^2 t_n^2} \sin\left(2\tau_n - \eta^{(n)}_\gamma - \eta^{(n)}_{\gamma'}\right). \tag{55}$$

For small q_n or τ_n, Eqs. 48 and 49 or Eqs. 50–55 become singular and can be set to zero.

These derivatives have to be augmented by Eq. (56) for the ring radius $R \equiv t_0$

$$\frac{\partial^2 R}{\partial \mathbf{r}_\beta \partial \mathbf{r}_{\beta'}} = \frac{1}{N^2 R} \mathbf{C}^{\beta'-\beta} - \frac{1}{N^4 R^3} \left(\sum_{\beta''} \mathbf{C}^{\beta''-\beta} \mathbf{r}_{\beta''} \right) \otimes \left(\sum_{\beta''} \mathbf{C}^{\beta''-\beta'} \mathbf{r}_{\beta''} \right). \tag{56}$$

The second sum on *rhs* of Eq. (47) contains the terms

$$\frac{\partial^2 r^k_\beta}{\partial \mathbf{r}_\alpha \partial \mathbf{r}_{\alpha'}} = \left(\frac{\partial \mathbf{e}_k}{\partial \mathbf{r}_{\alpha'}}, \mathbf{I} \right) \delta_{\alpha\beta} + \left(\frac{\partial \mathbf{e}_k}{\partial \mathbf{r}_\alpha}, \mathbf{I} \right) \delta_{\alpha'\beta} + \left(\frac{\partial^2 \mathbf{e}_k}{\partial \mathbf{r}_\alpha \partial \mathbf{r}_{\alpha'}}, \mathbf{r}_\beta \right), \tag{57}$$

where the derivatives $\partial \mathbf{e}_k / \partial r^l_\alpha$ have been given in Eqs. (38), (41) and (45). Now only $\partial^2 \mathbf{e}_k / \partial r^l_\alpha \partial r^{l'}_{\alpha'}$ in Eq. (57) has to be derived further

$$\begin{aligned} \frac{\partial^2 \mathbf{e}_z}{\partial \mathbf{r}_\alpha \partial \mathbf{r}_{\alpha'}} = \frac{1}{|\mathbf{R}' \times \mathbf{R}''|} \Big[& \mathbf{I} \times \mathbf{I} \sin(\eta_\alpha - \eta_{\alpha'}) - \frac{\partial \mathbf{e}_z}{\partial \mathbf{r}_\alpha} (\mathbf{e}_z, \mathbf{a}_{\alpha'}) \\ & - \frac{\partial \mathbf{e}_z}{\partial \mathbf{r}_{\alpha'}} (\mathbf{e}_z, \mathbf{a}_\alpha) - \mathbf{e}_z (\mathbf{e}_z, \mathbf{I} \times \mathbf{I}) \sin(\eta_\alpha - \eta_{\alpha'}) \\ & - \mathbf{e}_z \left(\frac{\partial \mathbf{e}_z}{\partial \mathbf{r}_\alpha}, \mathbf{a}_{\alpha'} \right) \Big], \end{aligned} \tag{58}$$

$$\begin{aligned} \frac{\partial^2 \mathbf{e}_x}{\partial \mathbf{r}_\alpha \partial \mathbf{r}_{\alpha'}} = \frac{1}{|\mathbf{u}|} \Big[& \left(\mathbf{e}_x, \frac{\partial \mathbf{u}}{\partial \mathbf{r}_{\alpha'}} \right) \frac{\partial \mathbf{e}_x}{\partial \mathbf{r}_\alpha} + \left(\mathbf{e}_x, \frac{\partial \mathbf{u}}{\partial \mathbf{r}_\alpha} \right) \frac{\partial \mathbf{e}_x}{\partial \mathbf{r}_{\alpha'}} \\ & + \mathbf{e}_x \left(\frac{\partial \mathbf{e}_x}{\partial \mathbf{r}_{\alpha'}}, \frac{\partial \mathbf{u}}{\partial \mathbf{r}_\alpha} \right) + \mathbf{e}_x \left(\mathbf{e}_x, \frac{\partial^2 \mathbf{u}}{\partial \mathbf{r}_\alpha \partial \mathbf{r}_{\alpha'}} \right) - \frac{\partial^2 \mathbf{u}}{\partial \mathbf{r}_\alpha \partial \mathbf{r}_{\alpha'}} \Big], \end{aligned} \tag{59}$$

$$\begin{aligned} \frac{\partial^2 \mathbf{e}_y}{\partial \mathbf{r}_\alpha \partial \mathbf{r}_{\alpha'}} = & \frac{\partial^2 \mathbf{e}_z}{\partial \mathbf{r}_\alpha \partial \mathbf{r}_{\alpha'}} \times \mathbf{e}_x + \frac{\partial \mathbf{e}_z}{\partial \mathbf{r}_\alpha} \times \frac{\partial \mathbf{e}_x}{\partial \mathbf{r}_{\alpha'}} \\ & + \frac{\partial \mathbf{e}_z}{\partial \mathbf{r}_{\alpha'}} \times \frac{\partial \mathbf{e}_x}{\partial \mathbf{r}_\alpha} + \mathbf{e}_z \times \frac{\partial^2 \mathbf{e}_x}{\partial \mathbf{r}_\alpha \partial \mathbf{r}_{\alpha'}}, \end{aligned} \tag{60}$$

where

$$\frac{\partial^2 \mathbf{u}}{\partial \mathbf{r}_\alpha \partial \mathbf{r}_{\alpha'}} = \frac{\partial \mathbf{e}_z^2}{\partial \mathbf{r}_\alpha \partial \mathbf{r}_{\alpha'}} \times \mathbf{R}' + \mathbf{c}_{\alpha\alpha'} + \mathbf{c}_{\alpha'\alpha}, \tag{61}$$

$$\mathbf{a}_\alpha = \mathbf{I} \times \mathbf{R}'' \sin \eta_\alpha - \mathbf{I} \times \mathbf{R}' \cos \eta_\alpha, \tag{62}$$

$$\mathbf{c}_{\alpha\alpha'} = \frac{\partial \mathbf{e}_z}{\partial \mathbf{r}_\alpha} \times \mathbf{I} \sin \eta_{\alpha'}, \tag{63}$$

and **u** has been defined in Eq. (6).

III. IMPLEMENTATION

The RPD coordinates and their derivatives have been programmed as a standalone program called RING in Fortran90, which is freely available via our CATCO web page http://smu.edu/catco/. The geometry optimization procedure in RPD coordinates for ring atoms and Z-matrix coordinates for substituents was implemented into the COLOGNE2019 program[50] through an integrated RING interface. The following two problems may be encountered.

- During geometry optimization, q_n or t_n often becomes negative, which may be converted to a positive one according to $\{q_n, \phi_n\} = \{-q_n, \phi_n \pm \pi\}$ and $\{t_n, \tau_n\} = \{-t_n, \tau_n \pm \pi\}$. This conversion is implemented only after the optimization procedure when printing results; it is not performed inside the optimization procedure since it may interfere with the structural extrapolation algorithms. The $q_{N/2}$ mode has no phase angle, and therefore both positive and negative values are possible.
- Substituent related bond angles may be difficult to define by regular Z-matrix coordinates due to the use of deformation coordinates. In Fig. 1, for example, five carbon atoms in planar C_5H_5 with C_{2v} symmetry have been defined by RPD coordinates, and then the Z-matrix coordinates of H1 cannot be defined since $\angle_{H1-C1-C2} = \angle_{H1-C1-C5} = 180° - \frac{1}{2}\angle_{C2-C1-C5}$, where $\angle_{C2-C1-C5}$ is not known. For this purpose, we designed a special indicator for the Z-matrix format, which specifies a dummy atom X1 at the midpoint between C2 and C5. Then the second dummy atom X2 in the same plane is defined by $\angle_{X1-C1-X2} = 90°$. With the help of X1 and X2, H1 may be easily specified in Z-matrix coordinates.

For the identification of the position of a given form in the $(N-3)$-dimensional puckering space, besides hypercylindrical coordinates $\{q_n, \phi_n\}$, hyperspherical coordinates $\{Q, \theta_n, \phi_n\}$ may also be used. For an N-ring with $N_q = N/2$ (N even) or $(N-1)/2$ (N odd), these coordinates are defined as

$$Q = \sqrt{\sum_{n=2}^{N_q} q_n^2}. \tag{64}$$

Using the symbol s_n ($n = 2, 3, \ldots, N_q - 1$) for the total puckering amplitude in a subspace,

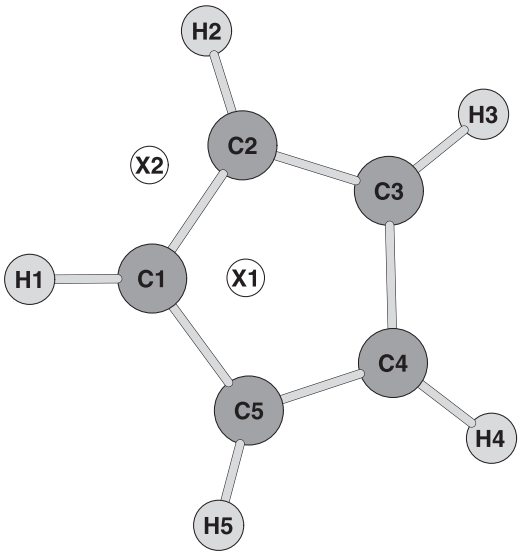

FIG. 1. Diagram of planar C_5H_5 in C_{2v} symmetry with two dummy atoms X1 and X2.

$$s_n = \sqrt{Q^2 - \sum_{i=2}^{n-1} q_i^2} = \sqrt{\sum_{i=n}^{N_q} q_i^2}, \tag{65}$$

a hyperspherical angle θ_n can be obtained according to

$$\theta_n = \frac{\pi}{2} - \arctan\left(\frac{s_n}{q_n}\right). \tag{66}$$

Therefore, for a given 8-ring form, the relative position between the $\{q_2, \phi_2\}$ space and the 1D q_4 space is determined by θ_2, and that between the $\{q_3, \phi_3\}$ space and the q_4 space by θ_3.

Similarly, one may define a total deformation amplitude

$$T = \sqrt{\sum_{n=1}^{N-2} t_n^2} \tag{67}$$

and the corresponding hyperspherical angle γ_n for planar deformation coordinates to form hyperspherical coordinates $\{T, \gamma_n, \tau_n\}$.

Test calculations were carried out for 5-, 6-, 7-, and 8-membered rings. Optimized amplitudes obtained via both analytical and numerical derivatives were in good agreement within 10^{-5} atomic units. Since 5- and 6-membered rings have been well studied in the literature, only 7- and 8-membered rings are discussed in this paper. For the purpose of demonstrating the advantages of using RPD coordinates, cycloheptane (C_7H_{14}) and cyclooctane (C_8H_{16}), were chosen as examples for odd and even N-rings, respectively. In this work, we focused on the puckering coordinates of cycloheptane and cyclooctane, since $Q \gg T$ in their conformers and deformation coordinates of planar cyclo[18]carbon (C_{18}), whereas the applications of RPD coordinates for smaller ring systems can be found in our early publications about puckering[25,39,41,51] and deformation coordinates.[22,23,40]

For cycloheptane and cyclooctane, geometry optimization and frequency calculations were carried out in Cartesian coordinates at the second order Møller–Plesset perturbation theory (MP2) level with Dunning's cc-pVTZ basis set,[52] whereas the smaller cc-pVDZ basis set was used for scanning the potential energy surface (PES) or for exploring the potential energy curve (PEC) by constrained optimization in RPD coordinates where the fixed geometric parameters may be determined by the common symmetry. DFT (density functional theory such as B3LYP[53,54]) calculations as well as CCSD(T) (coupled cluster theory with all single, double, and perturbative triple excitations) were also performed.

For cyclo[18]carbon, all calculations were performed with the DFT M06-2X hybrid functional[55] utilizing the def2-TZVPP basis set.[56] According to Ref. 57, this functional reproduces minimum and transition state conformers of cyclo[18]carbon correctly.

The Gaussian16[58] and COLOGNE2019[50] program packages were used for the calculations in Cartesian and RPD coordinates, respectively, whereas the CFOUR program[59] was used for CCSD(T) calculations.

IV. RESULTS AND DISCUSSION

A. Results for cycloheptane

As an odd-membered ring, cycloheptane does not possess a strain-free conformation.[60] Hendrickson[61] showed in 1967 that

cycloheptane has four stationary conformers: boat (**B**), chair (**C**), twist boat (**TB**), and twist chair (**TC**), in which **TC** is the lowest minimum state whereas **C** and **TB** are merely transition states.[62] Eight years later, Strauss and co-workers[63] found two additional transition states, i.e., bent transition state (**BTS**) and twist transition state (**TTS**; also called T3 by Wiberg[62]). These six conformers of cycloheptane and a less relevant planar one (**P**) with D_{7h} symmetry were recalculated at the MP2/cc-pVTZ level in this work. The results are collected in Table I (see also the supplementary material for their Cartesian and RPD coordinates with all possible ϕ_n angles). It should be noted that the calculation of **B** and **TB** with DFT is problematic. For example, both conformers are transition states according to B3LYP with small imaginary frequencies, but become minima with other functionals according to our test calculations.

The data in Table I reveal that cycloheptane has two minima (**TC** and **B**) and five transition states (**C**, **TB**, **BTS**, **TTS**, and **P**). The number of imaginary frequencies characterize **BTS** as a second-order transition state and **P** as the fourth order transition state. Inspecting the RPD coordinates of these conformers, we found that their $\{q_2, \phi_2\}$ puckering coordinates are significantly different, and thus may be used to distinguish them and to describe their relationship. As shown in Table S1, the period of ϕ_2 is $\frac{3}{7}\pi$ ($\approx$77.1°), which is not an integer divisor of 2π, and therefore $\frac{1}{3}\phi_2$ has to be taken instead. The PES in the $\{q_2, \frac{1}{3}\phi_2\}$ space was optimized at the MP2/cc-pVDZ level, where all the other coordinate parameters were relaxed.

As shown in Fig. 2, the six conformers except **P** can be grouped into two families. The proper conformers **C**, **BTS**, and **B** with C_s symmetry are in the $\phi_2 = 3m\pi/7$ ($m = 0, 1, \ldots, 13$) directions, while the twist conformers **TC**, **TTS**, and **TB** with C_2 symmetry are in the $3(m + \frac{1}{2})\pi/7$ directions. The other geometries on the PES have C_1 symmetry. Obviously, in the radical direction, **BTS** is a transition state between **C** and **B**, and **TTS** a transition state between **TC** and **TB**. Wiberg[62] surmised that **TTS** is an intermediate transition state between **TC** and **B**, which seems not to be true according to our results.

TC is the global minimum with the lowest energy, with the **C** conformer only 1.24 kcal/mol higher in energy allowing for a pseudorotation between **TC** and **C**, where **C** is a first order transition state. The **B** and **TB** conformers are about 3 kcal/mol higher in energy than **TC**. **B** and **TB** have very similar RPD amplitudes and the largest total puckering amplitude Q. Energetically, they can also pseudorotate freely with an energy difference of merely 0.01 kcal/mol, in which **B** is a local minimum and **TB**, a first order transition state. Between **TC** (**C**) and **TB** (**B**), the energy barrier of **TTS** (**BTS**) is relatively higher than the ones in the angular direction, so the **TC**–**C** and **TB**–**B** pseudorotations are more easily to happen. It is extremely unlikely to pass through the **P** conformer, a fourth order transition state being about 54 kcal/mol higher in energy than **TC**.

B. Results for cyclooctane

Cyclooctane is one of the most investigated ring molecule. During the last 50 years, it was studied using vibrational spectroscopy,[64,65] nuclear magnetic resonance (NMR)-spectroscopy,[66] and electron diffraction analysis.[67] Computational investigations were first based on force field calculations,[43,61,68–70] and only in the last 30 years *ab initio* quantum chemical calculations followed.[62,71,72] The conformational space of cyclooctane has been studied using *Distance Geometry*,[73] its properties in bulk liquid liquid phases were investigated with the help of molecular dynamics simulations,[74] extending these studies to the Monte Carlo level.[75] The conformers of cyclooctane have been also characterized employing Bayesian methods[76] or testing new methods for the loop closure problem.[77] The 72-dimensional hyperspace of cyclooctane was successfully reduced to a 2D CES.[78,79] Recently, the topological energy and conformational landscape of cyclooctane was explored[80,81] involving machine learning techniques.[82]

Many of these studies based their choice of conformers to be discussed on the pioneering work of Hendrickson who carried out in the mid 1960s, extensive studies on medium-seized rings using force field methods.[61,68,69] He identified ten different conformers of cyclooctane and tried to order them in different spaces and pseudorotational pairs. However, his analysis was hampered by the use of dihedral angles and the inherent redundancy problem, which led to ten basis conformations. Hence, most of the following studies of cyclooctane used Hendrickson's 10 *canonical forms*. This choice was supported by the 2D CES derived by Martin and co-workers and the dynamic processes these authors singled out on this CES.[79] The CES was found to be best described by the intersection of a sphere and a Klein bottle where the low dimensionality was obtained by a decomposition of the Klein bottle into two Möbius strips. This presentation may be quite useful, but is plagued by the fact that the conformational description is carried out with torsional angles, which is problematic when defining the unique forms of cyclooctane.

TABLE I. Stationary points of cycloheptane, MP2/cc-pVTZ calculations.

No.	Form	Sym.	ΔE (kcal/mol)	Q (Å)	T (Å)	R (Å)	q_2 (Å)	q_3 (Å)	θ_2 (deg)	Imag. freq. (cm^{-1})
1	TC	C_2	0.00	0.849	0.099	1.621	0.547	0.649	40.1	min.
2	C	C_s	1.24	0.803	0.084	1.634	0.460	0.658	35.0	$113i$ (a'')
3	B	C_s	2.95	1.173	0.120	1.554	1.173	0.015	89.3	min.
4	TB	C_2	2.96	1.172	0.120	1.554	1.172	0.012	89.4	$20i$ (b)
5	TTS	C_2	8.20	1.060	0.137	1.584	1.015	0.304	73.3	$218i$ (a)
6	BTS	C_s	12.20	0.963	0.112	1.621	0.914	0.302	71.7	$263i$(a'), $135i$ (a'')
7	P	D_{7h}	53.54	0.000	0.000	1.789	0.000	0.000	90.0	$416i$ (e_3''), $257i$ (e_2'')

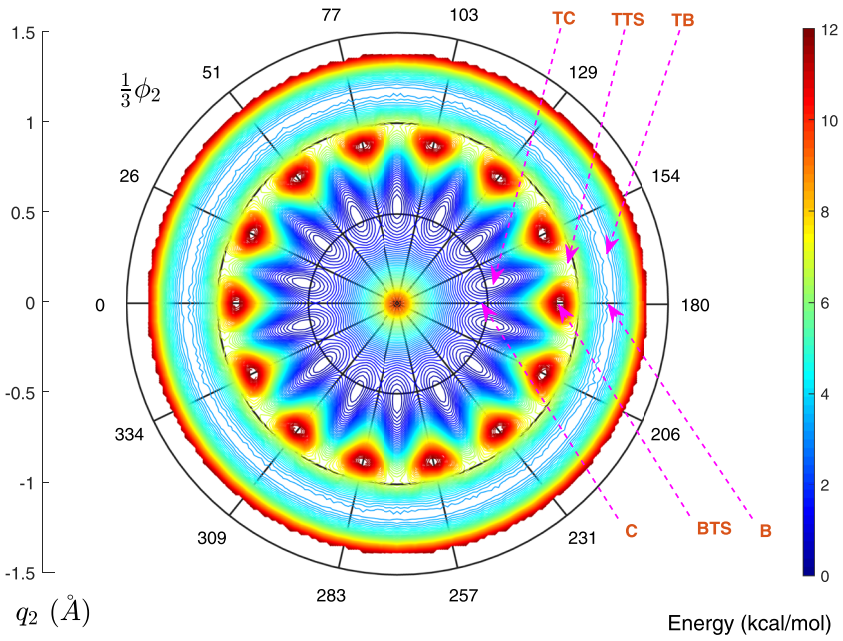

FIG. 2. PES and stationary points of cycloheptane in the $\{q_2, \frac{1}{3}\phi_2\}$ space. Note that at the center with q_2 = 0 Å, the $\{q_3, \phi_3\}$ coordinates are relaxed, so it is not the planar form *P*.

Before analyzing cyclooctane in terms of puckering coordinates, it is useful to summarize all its stationary conformers reported in the literature, which are much more complex than those of cycloheptane. Hendrickson's 10 conformers[61,68] are boat–chair (**BC**), chair–chair (**CC**), boat–boat (**BB**; also called "saddle"[61] but the latter name was not generally accepted[60]), twist chair (**TC**), chair (**C**), boat (**B**), crown (**CR**), twist chair–chair (**TCC**), twist boat–chair (**TBC**), and a "S4" conformer (denoted as **S** to distinguish from its S_4 point group symmetry). However, several of them were questioned in subsequent studies.

- **S**. Wiberg[62] showed that the **S** conformer was indeed, **BB** after optimization with B3LYP, but the existence of **S** is confirmed in Ref. 72 by Hartree–Fock (called the "B" conformer by mistake as pointed by Wiberg[62]) and also in this work using MP2/cc-pVTZ.
- **CC** and **TCC**. Rocha *et al.*[72] pointed out that the **CC** and **TCC** conformers do not exist at all at the Hartree–Fock level, which is also supported in this work by DFT calculations with different functionals. MP2 results are quite different: **TCC** exists if the basis set is large enough (e.g., 6-311†G* by Wiberg[62] and cc-pVTZ in this work), whereas **CC** may be obtained only with smaller Pople basis sets such as 3-21G and 6-311G, but turns into **CR** after geometry optimization with larger basis sets like 6-311††G**, cc-pVDZ, cc-pVTZ, etc. We also performed CCSD(T)/6-311G and CCSD(T)/cc-pVDZ calculations in this work to confirm the existence of **CC** and **TCC**, but even higher levels of calculations may be needed to further confirm them.

Apart from the well-known ten conformers of Hendrickson, other conformers were reported in the literature and also found in this work.

- **TB**. Hendrickson's **S** conformer was also named twist-boat (TB),[73,76,79,83,84] but in early work,[73,83] the geometry of TB appears to be quite different from that of the known S conformer although being of S_4 symmetry. Therefore, this **TB** conformer should be better considered as a new stationary geometry of cyclooctane. This new **TB** conformer has also been reported by Rocha *et al.*, called TS1.[72]
- **WT1**, **WT2**, and **WT4**. Wiberg calculated four new transition states at the MP2 level of theory (i.e., TS*n*, *n* = 1, 2, 3, and 4, denoted as WT*n* in this work), in which **WT2** is the same as the TS2 conformer by Rocha *et al.*,[72] whereas WT3 is identical to TC according to the RPD coordinate analysis of their coordinates.
- **NTn** (n = 1, 2, . . ., 7). In this work, seven new transition states were identified with the help of RPD coordinates, denoted as **NTn**; among them, **NT3** resembles the "peak" conformer of Martin *et. al.*[79] However, these authors did not provide coordinates for an additional analysis via RPD coordinates.
- **P**. A planar conformer (**P**) with D_{8h} symmetry is a high-order transition state with high energy. Different from the **P** conformer of cycloheptane, here, **P** plays a certain role since the D_{8h} point group has more subgroup symmetries than D_{7h}.

All 22 conformers, including the uncertain **CC** are summarized in Table II. Cartesian and RPD coordinates are collected in the supplementary material with all possible ϕ_n angles. Since q_4 changes its sign by the inversion operation of Cartesian coordinates, only positive q_4 values are reported. Table II shows that cyclooctane has five minima in which **BC** is the most stable one, being in agreement with previous studies.

TABLE II. Stationary points of cyclooctane, MP2/cc-pVTZ calculations.

No.	Form	Sym.	ΔE (kcal/mol)	Q (Å)	T (Å)	R (Å)	q_2 (Å)	q_3 (Å)	q_4 (Å)	θ_2 (deg)	θ_3 (deg)	Imag. freq. (cm^{-1})
1	BC	C_s	0.00	1.253	0.156	1.743	1.052	0.587	0.345	57.1	120.4	min.
2	TBC	C_2	1.73	1.123	0.169	1.767	0.720	0.833	0.220	39.9	104.8	min.
3	TCC	D_2	2.46	0.902	0.157	1.819	0.434	0.000	0.790	28.8	0.0	min.
4	CR	D_{4d}	2.52	0.808	0.000	1.853	0.000	0.000	0.808	0.0	0.0	min.
5	NT7	D_2	2.53	0.831	0.071	1.845	0.202	0.000	0.806	14.1	0.0	$29i$ (a)
6	S	S_4	2.83	1.595	0.172	1.660	1.595	0.000	0.000	90.0	90.0	min.
7	WT2	C_1	2.95	1.190	0.143	1.761	0.907	0.719	0.276	49.7	111.0	$114i$ (a)
8	BB	D_{2d}	3.43	1.518	0.166	1.693	1.518	0.000	0.000	90.0	90.0	$63i$ (a_2)
9	CC[a]	C_{2v}	4.07	0.866	0.083	1.859	0.225	0.000	0.836	15.1	0.0	$55i$ (a_2)
10	C	C_{2h}	9.51	0.944	0.200	1.804	0.000	0.944	0.000	0.0	90.0	$148i$ (a_u), $28i$ (a_g)
11	TC	C_{2h}	9.53	0.953	0.209	1.800	0.000	0.953	0.000	0.0	90.0	$20i$ (b_g)
12	WT4	C_s	9.71	1.447	0.183	1.709	1.420	0.243	0.139	78.8	119.7	$259i$ (a'), $41i$ (a'')
13	NT2	C_s	10.93	0.974	0.163	1.812	0.385	0.876	0.180	23.3	101.6	$181i$ (a''), $124i$ (a')
14	WT1	C_2	11.36	1.254	0.225	1.748	1.138	0.274	0.449	65.2	31.4	$169i$ (a)
15	TB	D_2	11.83	1.633	0.177	1.657	1.630	0.000	0.107	86.3	0.0	$105i$ (b_1)
16	B	D_{2d}	12.03	1.648	0.151	1.660	1.648	0.000	0.000	90.0	90.0	$185i$ (a_2), $61i$ (b_1)
17	NT6	C_2	12.58	1.538	0.208	1.680	1.519	0.125	0.208	80.9	148.9	$136i$ (a)
18	NT5	D_2	13.48	1.432	0.228	1.707	1.396	0.000	0.316	77.2	180.0	$145i$ (b_3), $140i$ (a)
19	NT4	C_s	14.77	1.010	0.165	1.819	0.767	0.338	0.562	49.5	31.0	$284i$ (a'), $87i$ (a'')
20	NT1	C_2	22.74	1.239	0.204	1.768	1.134	0.500	0.000	66.2	90.0	$341i$ (b), $195i$ (a)
21	NT3	C_{2v}	26.03	1.188	0.167	1.809	1.143	0.000	0.324	74.2	0.0	$302i$ (b_1), $266i$ (a_1), $126i$ (a_2)
22	P	D_{8h}	88.36	0.000	0.000	2.040	0.000	0.000	0.000	90.0	90.0	$489i$ (b_{2u}), $422i$ (e_{3g}), $240i$ (e_{2u})

[a]Uncertain conformer. Optimized at the MP2/6-311G level of theory.

Traditionally, the conformers of cyclooctane and their equivalent steric configurations are difficult to distinguish by merely using their energies, bond lengths, bond angles, and dihedral angles. However, this becomes now much easier by comparing their RPD amplitudes. Furthermore, a large number of equivalent configurations can be classified by different combinations of RPD phase angles (see Table S2).

There are only $N - 3 = 5$ unique types of out-of-plane displacements and $2N - 3 = 13$ planar ones in an 8-membered ring, if one starts with the **P** conformer as a suitable reference.[22,24,28,32] To investigate the relationship between the 22 conformers, the CES in the 5D puckering space is at first projected onto the 2D $\{q_2, q_3\}$ subspace, since q_2 and q_3 are the two most significantly different RPD coordinates. The PES at the MP2/cc-pVDZ level is plotted in Fig. 3 with different constraints of ϕ_2, ϕ_3, and q_4 to maintain a common symmetry higher than C_1. It should be noted that in Figs. 3(a) and 3(b), the maxima at about $\{q_2 = 0$ Å, $q_3 = 0.5$ Å$\}$ are not stationary points since they do not lead to a high symmetry C_{2h}. One can see in Figs. 3(a) and 3(b) that the PESs around $q_3 = 0$ Å are very flat, but since a smaller basis set cc-pVDZ being used, **TCC** and **NT7** cannot be located. The situation for **CC** is similar. Nevertheless, 19 conformers and their relationships can be described by Fig. 3. Three conformers are still missing, including **B**, **S**, and **WT2**.

The PESs in the $\{q_2, q_4\}$ subspace with different constraints of ϕ_2 and q_3 are plotted in Fig. 4, and the pure $\{q_n, \phi_n\}$ ($n = 2$ or 3) subspace in Fig. 5, where **B** and **S** may be located. The lowest pseudorotation paths connecting 21 conformers (except **P**) are, respectively, projected on q_2, q_3, ϕ_2, and ϕ_3, as shown in Fig. 6. **WT2** has only C_1 symmetry, i.e., no geometric constraint. Thus, as shown in Fig. 5(a), if all the other coordinate parameters are relaxed except a given ϕ_2, **WT2** connecting two known conformers **BC** and **TBC** can be obtained, and the resulting 1D PEC is shown in Fig. 6(h). For other 2D subspaces (e.g., $\{\phi_3, \phi_4\}$) and geometric constraints, the common symmetry is always C_1, so they are the same as those shown in Fig. 6(h).

In the following, we discuss the relationship between the 22 conformers.

- As shown in Fig. 3(a), **NT2** is a transition state between **TC** and **BC**, denoted as **TC**–**NT2**–**BC**. Similarly, there are **BC**–**WT4**–**BB**, **BC**–**NT4**–**CC** or **BC**–**NT4**–**CR** (depending on the existence of **CC**), and **BB**–**NT3**–**CC** or **BB**–**NT3**–**CR**. In addition, **BC** may turn into another **BC** with $\phi_3 = 180°$ through **NT3**, i.e., **BC**–**NT3**–**BC′**, being energetically less favorable than the path **BC**–**WT4**–**BB**–**WT4′**–**BC′**. The **BC**–**WT4**–**BB** path was reported by Wiberg[62] and also by Martin *et al.*[79] Martin *et al.* further suggested[79] that **S** (called TB therein) is a transition state between **WT4** (called TS4) and **BB**, which does not seem to be true according to our results. It is noteworthy that if **CC** exists (e.g., at the MP2/6-311G level of theory), it will be lower in energy than **CR**, so **CC** will be to a local minimum, whereas **CR** a transition state. The lowest pseudorotation paths connecting these conformers may be found in Figs. 6(a) and 6(b).

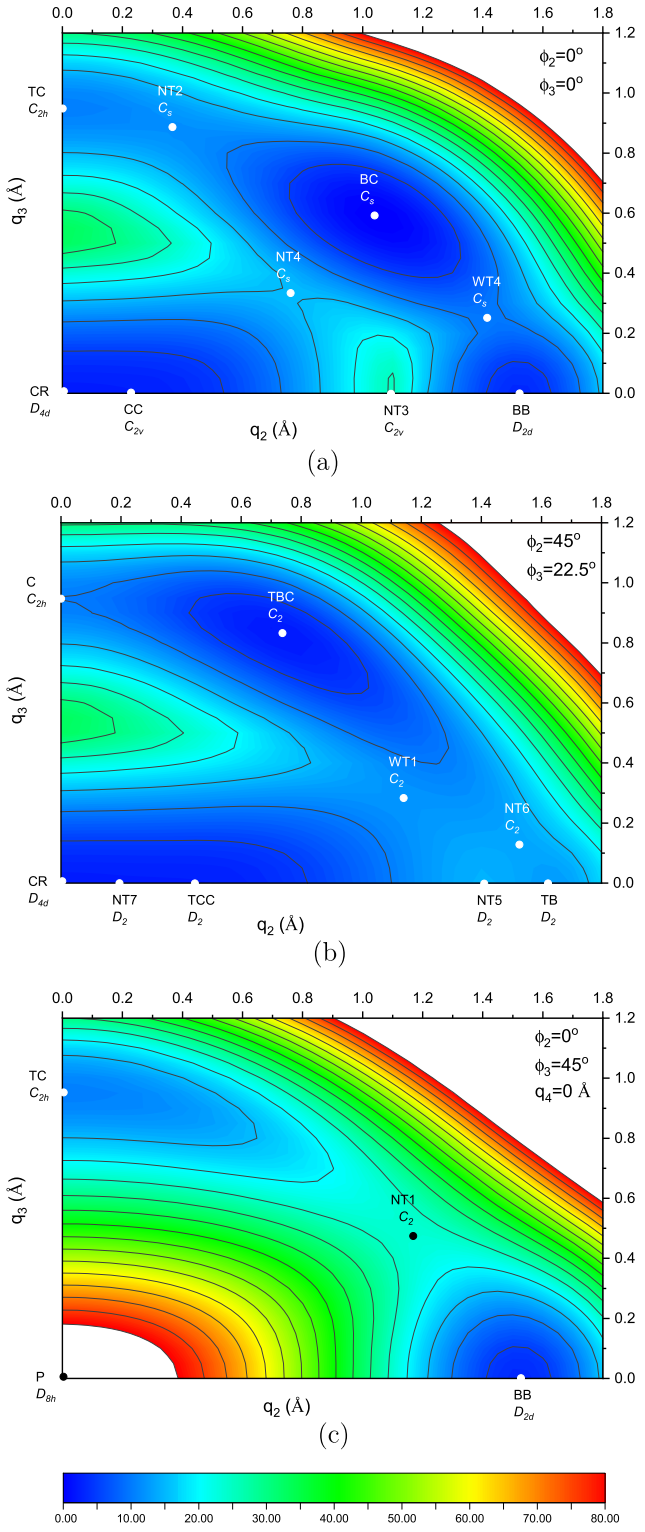

FIG. 3. PES and stationary points of cyclooctane in the $\{q_2, q_3\}$ space with (a) $\phi_2 = \phi_3 = 0°$, (b) $\phi_2 = 2\phi_3 = 45°$, and (c) $\phi_2 = 0°$, $\phi_3 = 45°$, and $q_4 = 0$ Å. CC, TCC, and NT7 cannot be obtained at the MP2/cc-pVDZ level.

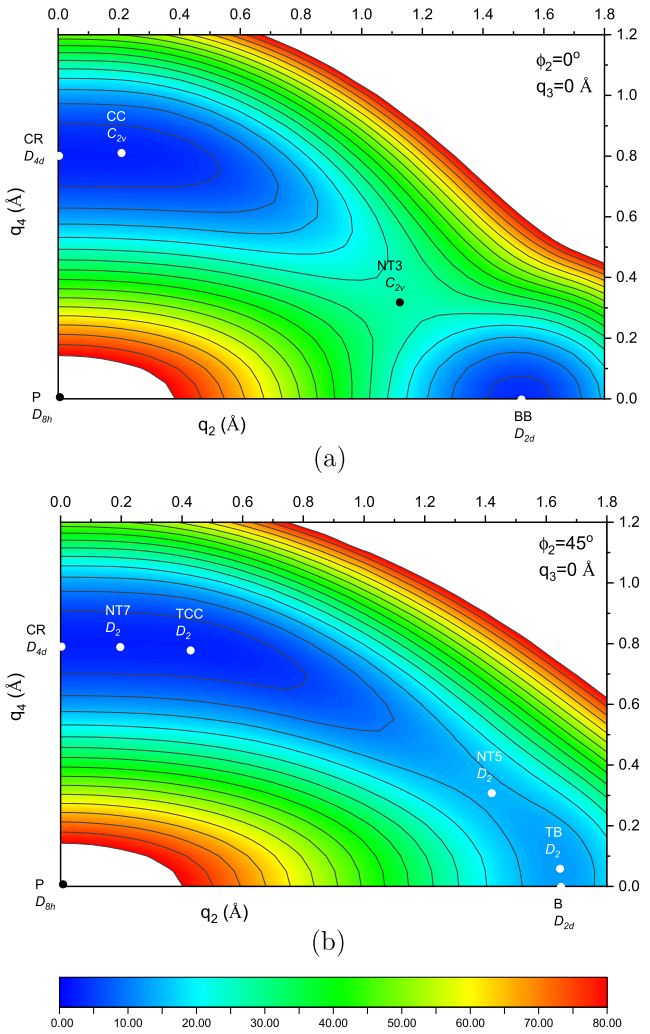

FIG. 4. PES and stationary points of cyclooctane in the $\{q_2, q_4\}$ space with (a) $\phi_2 = 0°$ and $q_3 = 0$ Å and (b) $\phi_2 = 45°$ and $q_3 = 0$ Å. CC, TCC, and NT7 cannot be obtained at the MP2/cc-pVDZ level.

- Figure 3(b) shows the **CR–NT7–TCC**, **TCC–NT5–TB**, **TBC–WT1–TCC**, **TBC–NT6–TB**, and **TBC–C–TBC′** (**TBC′**: **TBC** with $\phi_2 = 225°$) paths. In addition, paths **TBC–NT5–TBC″**, **TBC–NT6–TB–NT6′–TBC″**, and **TBC–WT1–TCC–WT1′–TBC″** (**TBC″**: **TBC** with $\phi_3 = 202.5°$) may also be possible, but the required energies are higher. Among these paths, the **TBC** (called TS1)–**WT1**–**TCC** path was also reported by Martin *et al.*,[79] whereas the path **TBC–WT1–CR** suggested by Wiberg[62] is only possible if **TCC** and **NT7** would not exist. The lowest pseudorotation paths connecting these conformers are plotted in Figs. 6(a) and 6(c).
- Figure 3(c) shows only one meaningful path, i.e., **TC–NT1–BB**. In addition, **TC** and **BB** may be connected to

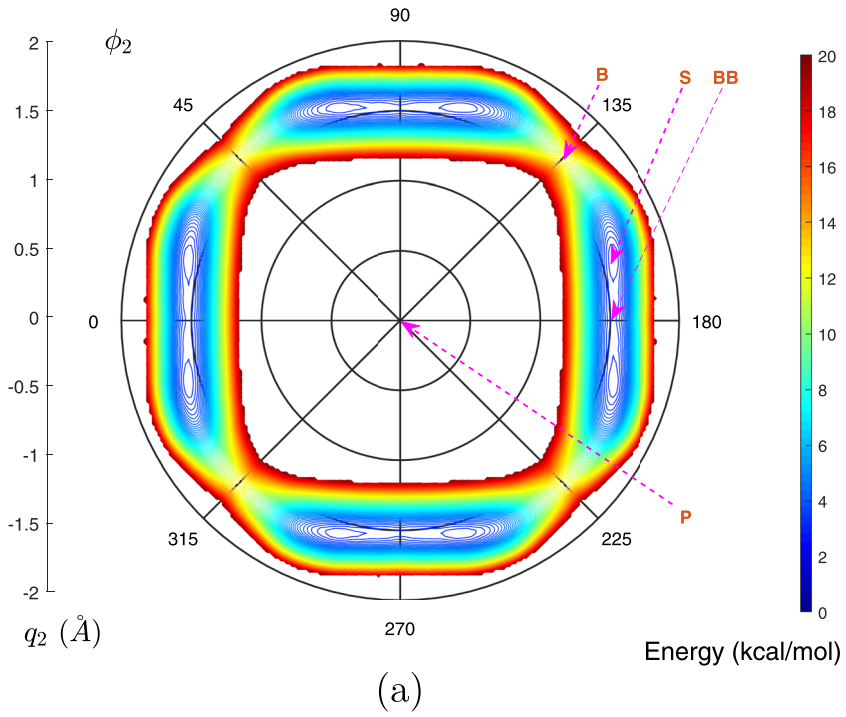

(a)

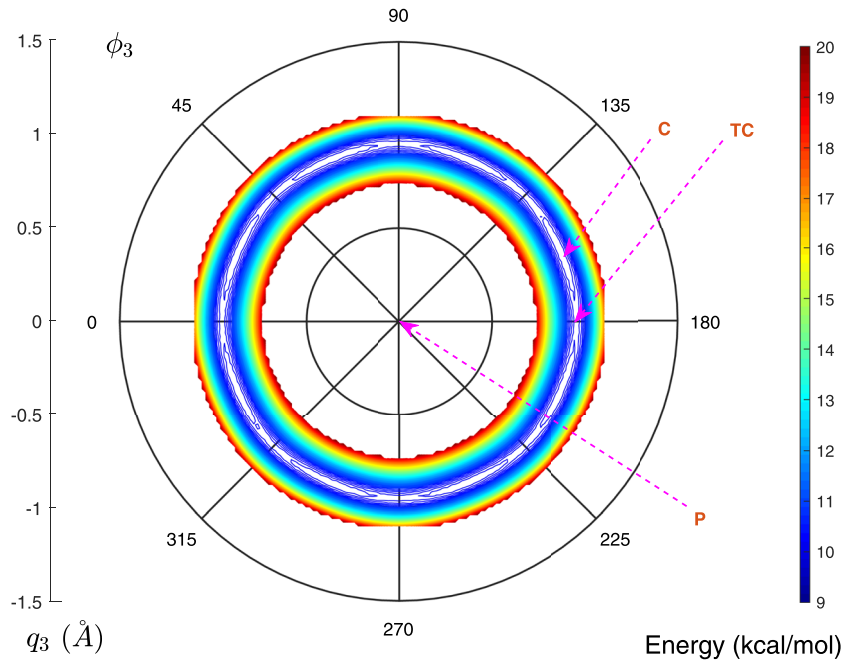

(b)

FIG. 5. PES and stationary points of cyclooctane in the (a) $\{q_2, \phi_2\}$ space in the S_4 common symmetry with $q_3 = q_4 = 0$ Å and (b) $\{q_3, \phi_3\}$ space in the C_i common symmetry with $q_2 = q_4 = 0$ Å.

their mirror image conformations through **P**, but the energy request would be too high, as seen in Fig. 6(d).

- In Fig. 4(a), there is **BB–NT3–CC** or **BB–NT3–CR** depending on the existence of **CC**, which has taken place in Fig. 3(a). The lowest pseudorotation paths connecting these conformers have been shown in Fig. 6(e).
- In Fig. 4(b) and also in Fig. 6(e), there are three paths, i.e., **TB–B–TB′** (**TB′**: **TB** with negative q_4), **CR–NT7–TCC**,

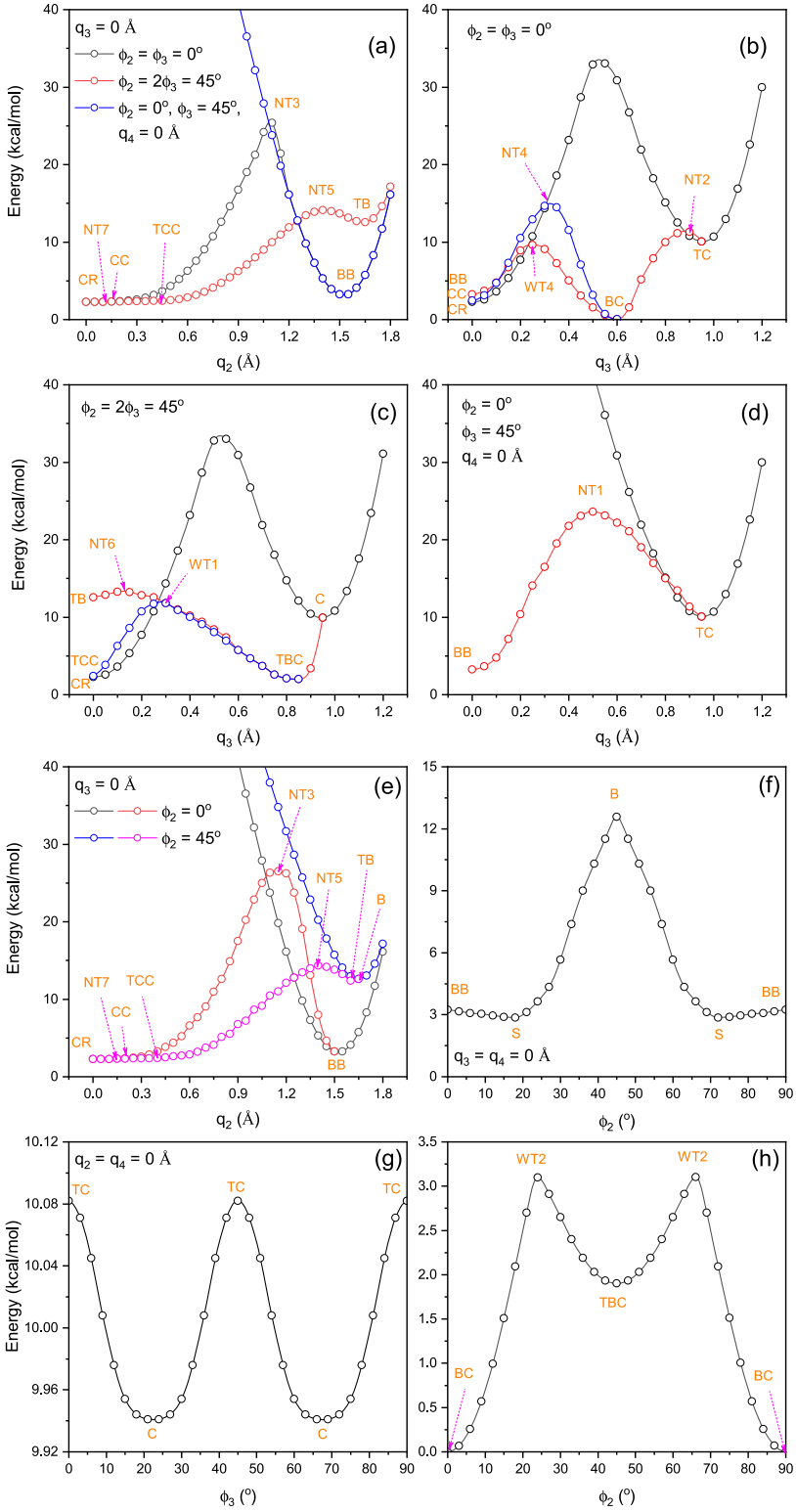

FIG. 6. One-dimensional PECs of the lowest pseudorotation path connecting stationary points of cyclooctane. (a) PECs along q_2 in the $\{q_2, q_3\}$ space, (b)–(d) PECs along q_3 in the $\{q_2, q_3\}$ space, (e) PECs along q_2 in the $\{q_2, q_4\}$ space, (f) PEC along ϕ_2 in the $\{q_2, \phi_2\}$ space, (g) PEC along ϕ_3 in the $\{q_3, \phi_3\}$ space, and (h) PEC along ϕ_2 without geometric constraints.

and **TCC**–**NT5**–**TB**, the latter two paths are also shown in Fig. 3(b).

- In Fig. 5(a), there are **S**–**BB**–**S′** and **S**–**B**–**S″**, where the possible ϕ_2 angles of **S**, **S′**, and **S″** may be found in Table S2. The $\{q_2, \phi_2\}$ pair spans the first pseudorotational space in the S_4 common symmetry with the two D_{2d}-symmetrical basis conformations **BB** and **B** at $m\pi/2$ (m = 0, 1, 2, and 3) and $(m + \frac{1}{2})\pi/2$, and **S** is a linear combination of **BB** and **B**. As assumed by Hendrickson, there are four **BB**, 4 **B**, and 8 **S** conformers along the ϕ_2 pseudorotation itinerary. Figure 6(f) shows the lowest pseudorotation path in detail.
- In Fig. 5(b), the **C** and **TC** conformers appear alternately (cf. Table S2 for possible ϕ_3 angles). The second pseudorotational space spanned by $\{q_3, \phi_3\}$ in the C_i common symmetry is defined by the C_{2h}-symmetrical **C** conformer at $(m + \frac{1}{2})\pi/4$ (m = 0, ..., 7) and **TC** at $m\pi/4$. There are 8 **C** and 8 **TC** conformers shown around the cycle. As seen in Fig. 6(g), the lowest pseudorotation path connecting **C** and **TC** is quite flat.
- As shown in Fig. 6(h), there is a **BC**–**WT2**–**TBC** path, which was also reported by Martin *et al.*,[79] Rocha *et al.*,[72] and Wiberg.[62]

According to Figs. 3–6, some of the paths previously reported in the literature are energetically and/or topologically not possible. For example, while the **TBC**–**TC** (called WT3 or TS3 therein)–**TBC′** path suggested by Wiberg[62] and also by Martin *et al.*[49] can be considered to be identical with our **TBC**–**C**–**TBC′** path, although **TC** and **C** are very close in energy, the **BC**–**TB** (TS1 therein)–**CR** suggested by Rocha *et al.*[72] cannot exist at all according to our calculations.

Compared to q_2, the puckering amplitude is generally more delocalized (or smaller) in q_3. The most delocalized puckering amplitude is found in q_4 for the **CR** conformer since an equally delocalized puckering (one atom up, the neighboring atom down) leads to the best staggering of the CH bonds in a cycloalkane. Hence, the total puckering amplitude Q has the smallest value for **CR** (Q = 0.808 Å, Table II) except **P** and becomes about 0.14 Å larger for **C** and **TC**, whereas it is 1.52–1.65 Å for **BB**, **S**, and **B**. As an important result, consequently, the way to get to **CR** from the $\{q_3, \phi_3\}$-space is much shorter than that from the $\{q_2, \phi_2\}$-space.

C. Results of Cyclo[18]carbon

In experimental[46] and advanced theoretical[57,85–89] studies, the planar cyclo[18]carbon molecule has two conformers, i.e., the polyyne minimum (**P**) with alternating weaker and stronger C–C bonds with D_{9h} symmetry and the cumulene transition structure (**C**) with identical C–C bonds with D_{18h} symmetry, being a good example to demonstrate the use of deformation coordinates.

An 18-membered ring has $N - 2 = 16$ pairs of $\{t_n, \tau_n\}$ deformation coordinates. For an arbitrary τ_n phase angle with a non-zero t_n amplitude, the resulting point group symmetry of the planar ring can be $C_{1h} \equiv C_s$ (n = 1, 5, 7, 11, and 13), C_{2h} (n = 2, 4, 8, 10, 14, and 16), C_{3h} (n = 3 and 15), C_{6h} (n = 6 and 12), and C_{9h} (n = 9). That is, m in C_{mh} is the greatest common divisor of N and n. By the definition of the deformation coordinates the $\{t_n, \tau_n\}$ modes squeeze an N-gon to an (N − n)-gon,[22] thus the 9-gon-like **P** form (assuming that the nine stronger C–C bonds are extremely short) must result from the $\{t_9, \tau_9\}$ modes; on the other hand, C_{9h} is the largest common subgroup of D_{9h} and D_{18h}. Therefore, $\{t_9, \tau_9\}$ are the dominant deformation modes. As demonstrated in Fig. 7, two basis forms are given by $\tau_9 = 90°$ (or 270°) and 0° (or 180°), respectively, where the former leads to a 9-gon-like configuration and the latter to a two-layer 9-gon-like one. Their deformation analysis shows that the two modes may be assigned to the normal vibrations in the b_{2u} and b_{1u} irreducible representations of D_{18h}, respectively (cf. Table A1 in the supplementary material of Ref. 22).

The PES calculated in the $\{t_9, \tau_9\}$ space is plotted in Fig. 8. During the optimization, all the other RPD amplitudes (except R) are fixed at zero since they may lead to higher energies with lower symmetries. At the M06-2X/def2-TZVPP level of theory, the **C** conformer is 9.42 kcal/mol higher in energy than the **P** conformer, being in good agreement with the results in Ref. 57. One can see in Fig. 8 that there are two orthogonal paths **P**–**C**–**P′** (**P′** is the **P** conformer in the 270° direction). One is in the radial direction with fixed $\tau_9 = 90°$ or 270° in the D_{9h} common symmetry, corresponding to the stretching of nine C_2 fragments (cf. Fig. 7) as reported in Ref. 57, which was also called the bond pseudolibration process.[40] The other path as indicated by the dotted blue curve in Fig. 8 corresponds to the bond pseudorotation process,[40] where each carbon atom β rotates by $\tau_n - \eta_\gamma^{(n)}$ on a small circle with the orbit radius t_9 (cf. Fig. 1 in Ref. 22 as a demonstration of 5-membered ring). In practice, the configuration of cyclo[18]carbon may be more complicated since it could be driven by a random combination of the two basic paths.

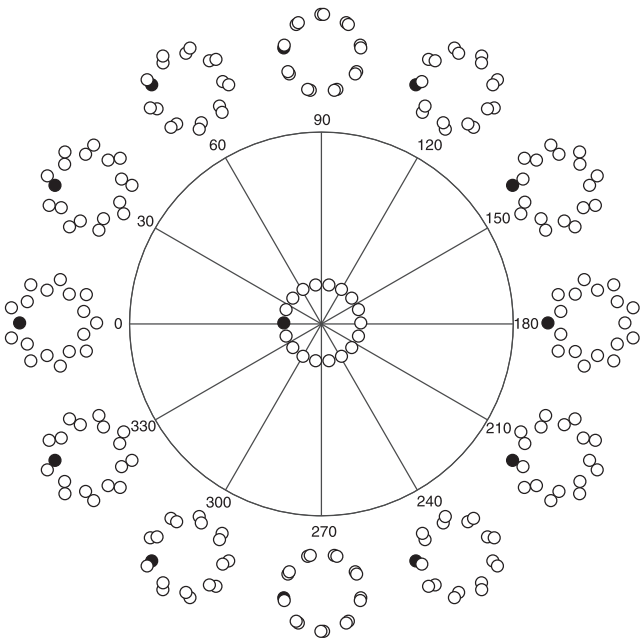

FIG. 7. Bond pseudorotation cycle in the $\{t_9, \tau_9\}$ space of a 18-gon with t_9 being extremely large and τ_9 increasing in a step of 30° from 0° to 360°. The position of atom 1 is indicated by a black dot (clockwise ordering of ring atoms).

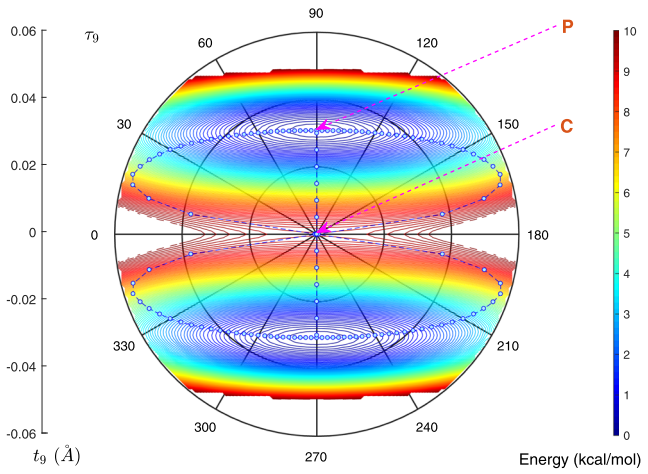

FIG. 8. PES of C_{18} spanned by $\{t_9, \tau_9\}$. The symmetries are D_{18h} at the center, D_{9h} in 0°, 90°, 180°, and 270° directions, and C_{9h} at other positions. The dotted blue curve indicates the lowest pseudorotation path connecting the P and C conformers.

V. CONCLUSIONS

In this work, we developed analytic gradient and second derivatives through B-matrices and D-tensors in terms of RPD coordinates; so constraint or full geometry optimizations for (poly)cyclic molecules in terms of RPD coordinates are now possible, particularly important for an optimization at non-stationary points, which is not feasible with Cartesian or internal coordinates. The application of RPD coordinates for the description of Berry pseudorotations, fullerene pseudorotations, etc. will be performed in future work.

SUPPLEMENTARY MATERIAL

All optimized stationary point geometries of C_7H_{14}, C_8H_{16}, and C_{18} in RPD and Cartesian coordinates are provided in the supplementary material.

ACKNOWLEDGMENTS

This work was financially supported by the National Science Foundation, Grant No. CHE 1464906. We thank SMU for providing generous computational resources. Dmitry Izotov is acknowledged for his preliminary programming work. W.Z. also acknowledges the financial support by the Double First-Class University Construction Project of Northwest University.

In memoriam of Dieter Cremer.

REFERENCES

[1] N. Vaidehi and A. Jain, J. Phys. Chem. B **119**, 1233 (2015).
[2] K. Nemeth, M. Challacombe, and M. van Veenendaal, J. Comput. Chem. **31**, 2078 (2010).
[3] E. B. Wilson, J. C. Decius, and P. C. Cross, *Molecular Vibrations* (McGraw-Hill, New York, 1955).
[4] G. Herzberg, *Molecular Spectra and Molecular Structure, II. Infrared and Raman Spectra of Polyatomic Molecules* (Van Nostrand, New York, 1945).
[5] F. Kalincsak and G. Pongor, Theor. Chem. Acc. **134**, 108 (2015).
[6] C. Puzzarini, J. Bloino, N. Tasinato, and V. Barone, Chem. Rev. **119**, 8131 (2019).
[7] E. Frezza and R. Lavery, J. Phys. Chem. B **123**, 1294 (2019).
[8] M. AlQuraishi, J. Comput. Chem. **40**, 885 (2019).
[9] H. Jung, R. Covino, and G. Hummer, arXiv:1901.04595 (2019).
[10] C. F. Jackels, Z. Gu, and D. G. Truhlar, J. Chem. Phys. **102**, 3188 (2015).
[11] M. Rey, J. Chem. Phys. **151**, 024101 (2019).
[12] V. Bakken and T. Helgaker, J. Phys. Chem. **117**, 9160 (2000).
[13] J. Baker, A. Kessi, and B. Delley, J. Chem. Phys. **105**, 192 (1996).
[14] Y.-Y. Chuang and D. G. Truhlar, J. Phys. Chem. A **102**, 242 (1998).
[15] C. Peng, P. Y. Ayala, H. B. Schlegel, and M. J. Frisch, J. Comput. Chem. **17**, 49 (1996).
[16] P. Pulay and G. Fogarasi, J. Chem. Phys. **96**, 2856–2860 (1992).
[17] B. Paizs, J. Baker, S. Suhai, and P. Pulay, J. Phys. Chem. **113**, 6566 (2000).
[18] H. B. Schlegel, Int. J. Quantum Chem., Quantum Chem. Symp. **44**(S26), 243 (1992).
[19] J. K. Watson, J. Mol. Struct. **695–696**, 71 (2004).
[20] J. Pesonen, K. O. E. Henriksson, J. R. López-Blanco, and P. Chacón, J. Math. Chem. **50**, 1521 (2012).
[21] J. R. Reimers, J. Chem. Phys. **115**, 9103 (2001).
[22] W. Zou, D. Izotov, and D. Cremer, J. Phys. Chem. A **115**, 8731 (2011).
[23] W. Zou, M. Filatov, and D. Cremer, Int. J. Quantum Chem. **112**, 3277 (2012).
[24] D. Cremer and J. A. Pople, J. Am. Chem. Soc. **97**, 1354 (1975).
[25] D. Cremer and K. J. Szabo, in *Conformational Behavior of Six-Membered Rings*, edited by E. Juaristi (Wiley VCH, Weinheim, 1995), pp. 59–135.
[26] R. S. Berry, J. Chem. Phys. **32**, 933 (1960).
[27] D. Ugi, H. Margiüarding, H. Klusacek, and P. Gillespie, Acc. Chem. Res. **4**, 288 (1971).
[28] D. Cremer, J. Phys. Chem. **94**, 5502 (1990).
[29] D. Cremer, Quantum Chemical Program Exchange **288**, 1 (1975).
[30] H. Essén and D. Cremer, Acta Crystallogr., Sect. B: Struct. Sci. **40**, 418 (1984).
[31] D. Cremer, J. Chem. Phys. **70**, 1898 (1979).
[32] D. Cremer, Isr. J. Chem. **20**, 12 (1980).
[33] D. Cremer, O. Dorofeeva, and V. Mastryukov, *8th Austin Symposium on Molecular Structure* (The University of Texas at Austin, 1980), Vol. 66, p. 1.
[34] D. Cremer, Fresenius' Z. Anal. Chem. **304**, 275 (1980).
[35] D. Cremer, O. Dorofeeva, and V. Mastryukov, J. Mol. Struct. **75**, 225 (1981).
[36] D. Cremer, in *Peroxides* (John Wiley & Sons, 1983), pp. 1–84.
[37] P. Schleyer, P. H. M. Budzelaar, D. Cremer, and E. Kraka, Angew. Chem., Int. Ed. **23**, 374 (1984).
[38] D. Cremer, B. Dick, and D. Christen, J. Mol. Struct.: THEOCHEM **110**, 277 (1984).
[39] A. Wu and D. Cremer, J. Phys. Chem. A **107**, 1797 (2003).
[40] W. Zou and D. Cremer, Aust. J. Chem. **67**, 435 (2014).
[41] M. K. Jahn, D. A. Dewald, M. Vallejo-López, E. J. Cocinero, A. Lesarri, W. Zou, D. Cremer, and J.-U. Grabow, Chem. Eur. J. **20**, 14084 (2014).
[42] S. Lyu, N. Beiranvand, M. Freindorf, and E. Kraka, J. Phys. Chem. A **123**, 7087 (2019).
[43] D. G. Evans and J. C. A. Boeyens, Acta Crystallogr., Sect. B: Struct. Sci. **44**, 663 (1988).
[44] A. D. Hill and P. J. Reilly, J. Chem. Inf. Model. **47**, 1031 (2007).
[45] L. Paoloni, S. Rampino, and V. Barone, J. Chem. Theory Comput. **15**, 4280 (2019).
[46] K. Kaiser, L. M. Scriven, F. Schulz, P. Gawel, L. Gross, and H. L. Anderson, Science **365**, 1299 (2019).
[47] W. Zou, R. Kalescky, E. Kraka, and D. Cremer, J. Chem. Phys. **137**, 084114 (2012).
[48] J. O. Lindner, K. Sultangaleeva, M. I. S. Röhr, and R. Mitrić, J. Chem. Theory Comput. **15**, 3450 (2019).
[49] H. B. Schlegel, Wiley Interdiscip. Rev.: Comput. Mol. Sci. **1**, 790 (2011).
[50] E. Kraka, W. Zou, M. Filatov, J. Gräfenstein, D. Izotov, J. Gauss, Y. He, A. Wu, V. Polo, L. Olsson, Z. Konkoli, Z. He, and D. Cremer, COLOGNE19, 2019.

[51] A. Wu, D. Cremer, A. A. Auer, and J. Gauss, J. Phys. Chem. A **106**, 657 (2002).
[52] T. Dunning, J. Chem. Phys. **90**, 1007 (1989).
[53] A. D. Becke, J. Chem. Phys. **98**, 5648 (1993).
[54] P. J. Stevens, F. J. Devlin, C. F. Chabalowski, and M. J. Frisch, J. Phys. Chem. **98**, 11623 (1994).
[55] Y. Zhao and D. Truhlar, Theor. Chem. Acc. **120**, 215 (2008).
[56] F. Weigend and R. Ahlrichs, Phys. Chem. Chem. Phys. **7**, 3297 (2005).
[57] G. V. Baryshnikov, R. R. Valiev, A. V. Kuklin, D. Sundholm, and H. Ågren, J. Phys. Chem. Lett. **10**, 6701 (2019).
[58] M. J. Frisch, G. W. Trucks, H. B. Schlegel, G. E. Scuseria, M. A. Robb, J. R. Cheeseman, G. Scalmani, V. Barone, G. A. Petersson, H. Nakatsuji, X. Li, M. Caricato, A. V. Marenich, J. Bloino, B. G. Janesko, R. Gomperts, B. Mennucci, H. P. Hratchian, J. V. Ortiz, A. F. Izmaylov, J. L. Sonnenberg, D. Williams-Young, F. Ding, F. Lipparini, F. Egidi, J. Goings, B. Peng, A. Petrone, T. Henderson, D. Ranasinghe, V. G. Zakrzewski, J. Gao, N. Rega, G. Zheng, W. Liang, M. Hada, M. Ehara, K. Toyota, R. Fukuda, J. Hasegawa, M. Ishida, T. Nakajima, Y. Honda, O. Kitao, H. Nakai, T. Vreven, K. Throssell, J. A. Montgomery, Jr., J. E. Peralta, F. Ogliaro, M. J. Bearpark, J. J. Heyd, E. N. Brothers, K. N. Kudin, V. N. Staroverov, T. A. Keith, R. Kobayashi, J. Normand, K. Raghavachari, A. P. Rendell, J. C. Burant, S. S. Iyengar, J. Tomasi, M. Cossi, J. M. Millam, M. Klene, C. Adamo, R. Cammi, J. W. Ochterski, R. L. Martin, K. Morokuma, O. Farkas, J. B. Foresman, and D. J. Fox, Gaussian 16 Revision B.1 (2016).
[59] J. F. Stanton, J. Gauss, L. Cheng, M. E. Harding, D. A. Matthews, and P. G. Szalay, "CFOUR: Coupled-cluster techniques for computational chemistry, a quantum-chemical program package," (2019), with contributions from A. A. Auer, R. J. Bartlett, U. Benedikt, C. Berger, D. E. Bernholdt, Y. J. Bomble, O. Christiansen, F. Engel, R. Faber, M. Heckert, O. Heun, M. Hilgenberg, C. Huber, T.-C. Jagau, D. Jonsson, J. Jusélius, T. Kirsch, K. Klein, W. J. Lauderdale, F. Lipparini, T. Metzroth, L. A. Mück, D. P. O'Neill, D. R. Price, E. Prochnow, C. Puzzarini, K. Ruud, F. Schiffmann, W. Schwalbach, C. Simmons, S. Stopkowicz, A. Tajti, J. Vázquez, F. Wang, and J. D. Watts, and the integral packages MOLECULE (J. Almlöf and P. R. Taylor), PROPS (P. R. Taylor), ABACUS (T. Helgaker, H. J. Aa. Jensen, P. Jørgensen, and J. Olsen), and ECP routines by A. V. Mitin and C. van Wüllen, for the current version, see http://www.cfour.de.
[60] V. Dragojlovic, ChemTexts **1**, 14 (2015).
[61] J. B. Hendrickson, J. Am. Chem. Soc. **89**, 7036 (1967).
[62] K. B. Wiberg, J. Org. Chem. **68**, 9322 (2003).
[63] D. F. Bocian, H. M. Pickett, T. C. Rounds, and H. L. Strauss, J. Am. Chem. Soc. **97**, 687 (1975).
[64] P. W. Pakes, T. C. Rounds, and H. L. Strauss, J. Phys. Chem. **85**, 2476 (1981).
[65] H. M. Pickett and H. L. Strauss, J. Chem. Phys. **55**, 324 (1971).
[66] F. A. L. Anet, "Dynamics of eight-membered rings in the cyclooctane class," in *Dynamic Chemistry*, Topics in Current Chemistry (Springer Verlag, Berlin, Heidelberg, 1974), Vol. 45, pp. 230–242.
[67] O. V. Dorofeeva, V. S. Mastryukov, N. L. Allinger, and A. Almenningen, J. Phys. Chem. **89**, 252 (1985).
[68] J. B. Hendrickson, J. Am. Chem. Soc. **86**, 4854 (1964).
[69] J. B. Hendrickson, J. Am. Chem. Soc. **89**, 7047 (1967).
[70] P. M. Ivanov and E. Osawa, J. Comput. Chem. **5**, 307 (1984).
[71] K. Siam, O. V. Dorofeeva, V. S. Mastryukov, J. D. Ewbank, N. L. Allinger, and L. Schäfer, J. Mol. Struct.: THEOCHEM **164**, 93 (1988).
[72] W. R. Rocha, J. R. Pilego, S. M. Resende, H. F. D. Santos, M. A. D. Oliveira, and W. B. D. Almeida, J. Comput. Chem. **19**, 524 (1998).
[73] P. K. Weiner, S. Opeta, G. Wipff, T. Havel, I. D. Kuntz, R. Langridge, and P. Kollman, Tetrahedron **39**, 1113 (1983).
[74] R. K. Bharadwaj, Mol. Phys. **98**, 211 (2000).
[75] Z. Chen and F. A. Escobedo, J. Chem. Phys. **113**, 11382 (2000).
[76] J. Perez, K. Nolsøe, M. Kessler, L. García, E. Perez, and J. L. Serrano, Acta Crystallogr., Sect. B: Struct. Sci. **61**, 585 (2005).
[77] J. M. Porta, L. Ros, F. Thomas, F. Corcho, J. Canto, and J. J. Perez, J. Comput. Chem. **28**, 2170 (2007).
[78] W. M. Brown, S. Martin, S. N. Pollock, E. A. Coutsias, and J.-P. Watson, J. Chem. Phys. **129**, 064118 (2008).
[79] S. Martin, A. Thompson, E. A. Coutsias, and J.-P. Watson, J. Chem. Phys. **132**, 234115 (2010).
[80] I. Membrillo-Solis, M. Pirashvili, L. Steinberg, J. Brodzki, and J. G. Frey, arXiv:1907.07770 (2019).
[81] S. Martin and J.-P. Watson, Comput. Geom. **44**, 427 (2011).
[82] B. Seo, S. Kim, M. Lee, Y.-W. Lee, and W. B. Le, J. Phys. Chem. C **122**, 23224 (2018).
[83] F. A. L. Anet and J. Krane, Tetrahedron Lett. **14**, 5029 (1973).
[84] J. Pérez, L. García, E. Pérez, J. L. Serrano, and M. Kessler, J. Mol. Struct. **1027**, 186 (2012).
[85] T. Torelli and L. Mitas, Phys. Rev. Lett. **85**, 1702 (2000).
[86] S. Arulmozhiraja and T. Ohno, J. Chem. Phys. **128**, 114301 (2008).
[87] E. Brémond, A. J. Pérez-Jiménez, C. Adamo, and J. C. Sancho-García, J. Chem. Phys. **151**, 211104 (2019).
[88] A. Nandi, E. Solel, and S. Kozuch, Chem. Eur. J. **26**, 625 (2020).
[89] T. Lu, Q. Chen, and Z. Liu, chemRxiv: 11320130.v1 (2019).